Applied Chemical Engineering (2024) Volume 7 Issue 3
doi: 10.59429/ace.v7i3.5509

RESEARCH ARTICLE

Effect of water matrix on sulfate radical behavior during BTB degradation by activated persulfate

Nedjma Lahmar[1], Mokhtar Djehiche[1,*], Alexandre Tomas[2], Marwa Bachiri[1], Samir Bouacha[1]

[1] *Inorganic Materials Laboratory, University Pole, Road Bordj Bou Arreridj, M'sila 28000 Algeria*

[2] *Institut Mines-Télécom Nord Europe, Univ. Lille, Center for Energy and Environment, F-59000, Lille, France*

***Corresponding author:** Mokhtar Djehiche, mokhtar.djehiche@univ-msila.dz

ABSTRACT

One of the primary constraints on the use of activated persulfate (PS), a precursor of the sulfate radical (SR), is a lack of understanding of its reaction pathways in the subsurface. SRs can degrade the target dye Bromothymol Blue (BTB) depending on several parameters, including the initial concentrations of PS and BTB, time, water salts (Cl^-, HCO_3^-, HPO_4^{2-}, SO_4^{2-}, NO_2^- and NO_3^-),cations (Na^+ and K^+), ionic strength, catalytic ions (Fe^{2+}, Ni^{2+}, Cu^{2+}, and Ag^+), and temperature. Experiments and numerical simulations using the established kinetic model yielded second-order rate constants for the reaction of BTB with the dominant SR at pH 3 of $(1.1 \pm 0.55) \times 10^8$, $((1.5 \pm 0.77) \times 10^8$, $(1.9 \pm 0.95) \times 10^8$ and $(2.2 \pm 1.1) \times 10^8$ M^{-1} s^{-1} at 40, 50, 60, and 70°C, respectively. These rate constants were used to calculate the kinetic activation parameters (E_a, $\Delta H^{\neq}$, $\Delta S^{\neq}$, $\Delta G^{\neq}$) according to the Arrhenius and Eyring equations. The results obtained are as follows: 19.8 kJ mol^{-1}, 16.36 kJ mol^{-1}, - 0.038 kJ mol^{-1} K^{-1}, and 27.78 kJ mol^{-1}. Finally, a possible mechanism for the discoloration of BTB by SR is proposed, in which the destruction of aromatic ring structures occurs alongside the discoloration of BTB.

Keywords: bromothymol blue; activated persulfate; discoloration; water matrix; transition metals; temperature; and kinetics

ARTICLE INFO

Received: 22 June 2024
Accepted: 26 July 2024
Available online: 29 August 2024

1. Introduction

With a global production of one million tons, dyes are used by small and large industries worldwide, particularly in the tanning, food, cosmetics, textile, and medical sectors[1]. These contaminants are of concern because of their persistence, bioaccumulation, and environmental and health consequences[2–4]. BTB is a sulfonphthalein-based dye used as an acid-base indicator in a wide range of industries, including textiles, pharmaceuticals, cosmetics, plastics, paint, ink, photography, and paper[5]. This compound has been extensively researched in a variety of disciplines, including analytical chemistry, biochemistry, microbiology, and ecology [6–8]. Prolonged exposure to BTB can irritate the respiratory system, skin, eyes, and nasal passages while also posing a risk to the liver, kidneys, and heart[9].

Furthermore, BTB is a primary water and soil pollutant that is highly resistant to degradation techniques and does not decompose directly through oxidation[10]. Pollutants, including BTB, are typically removed using oxidation processes like the Fenton effect and in situ chemical oxidation. Activated PS treatment is commonly used to remediate groundwater and the environment by destroying contaminants[11,12] using radical-based processes[2,13] or direct electron transfer[14]. The radical process (Eq. 1) involves breaking the O-O bond in PS, producing active species like SR and hydroxyl radical ($OH^•$) [15,16]. In basic conditions, the latter is the predominant radical, whereas in acidic conditions, the

former is dominant[15,17–19]. In fact, SRs work effectively across a wider pH range, from 3 to 10[20]. They also allow for the rapid and non-selective oxidation of organic pollutants[21,22].

$$S_2O_8^{2-} \xrightarrow{Activator} SO_4^{\cdot-} + \cdots \quad (1)$$

PS decomposes when exposed to heat[13,23], transition metals[24,25], ultraviolet (UV) light[26–28], and other means[29–33]. Thermal activation of PS was one of the first methods used for this purpose because it does not require expensive catalysts and only requires basic equipment[34]. Numerous studies have proposed various solutions for reducing the process's environmental and energy footprint, such as using heat or steam cogeneration on an industrial scale[35] or coupling with a renewable energy source such as sunlight[36] and solar thermal energy[37,38]. In a reaction mixture, the thermal decomposition of PS ions (heat activation) results in the formation of two SR (Eq. 2), which react with PS anions (Eq. 3), water (Eq. 4), self-reaction (Eq. 5), and organic compounds (BTB in our case) (Eq. 6) [12,39–41]:

$$S_2O_8^{2-} + \text{Heat} \rightarrow 2\,SO_4^{\cdot-} \quad (2)$$

$$S_2O_8^{2-} + SO_4^{\cdot-} \rightarrow S_2O_8^{\cdot-} + SO_4^{2-} \quad (3)$$

$$SO_4^{\cdot-} + H_2O \rightarrow OH^{\cdot} + H^+ + SO_4^{2-} \quad (4)$$

$$SO_4^{\cdot-} + SO_4^{\cdot-} \rightarrow S_2O_8^{2-} \quad (5)$$

$$SO_4^{\cdot-} + \text{BTB} \rightarrow \text{Product} \quad (6)$$

Temperature is the key parameter in this process, with most studies ranging from 20 to 70°C, but the most efficient processes have been reported at temperatures of at least 60°C [42]. The corresponding activation energy ranges between 128.48 and 140.16 kJ mol^{-1}[43]. The rise in temperature causes secondary reactions due to the non-productive decomposition of PS, as well as an increase in energy consumption[44,45]. PS can also be activated through electron transfer with metals[46,47], such as cobalt, silver, manganese, and iron. This process results in the formation of SRs (Eq. 7), where Mn^{n+} represents typical metal ions:

$$S_2O_8^{2-} + Mn^{n+} \rightarrow Mn^{n+1} + SO_4^{\cdot-} + SO_4^{2-} \quad (7)$$

The use of metal ions raises practical concerns, particularly about recycling and secondary pollution. Nonetheless, iron ions and their oxides have been extensively researched because they are environmentally friendly, non-toxic, and inexpensive[48]. Inorganic anions found in water and wastewater include chlorides (Cl^-), bicarbonates (HCO_3^-), phosphates (HPO_4^{2-}) nitrates (NO_3^-), nitrites (NO_2^-) and sulfates (SO_4^{2-}). These anions can act as radical scavengers[49], causing less reactive complexes to form. They occasionally produce toxic intermediates and byproducts [50,51]. These anions can have a wide range of effects on the degradation of organic pollutants, from beneficial to detrimental. This is dependent on the species to be degraded and their concentrations in the wastewater. For example, low chloride ion concentrations inhibited the degradation of triclosan and chloroxylenol, whereas increasing concentrations favored degradation[43]. In other studies, Cl^- ions promote benzotriazole degradation at concentrations less than 10 mM, whereas 100 mM inhibits it[52].Thus, rather than generalizing this effect, it is more appropriate to investigate the effect of these anions on the degradation of each organic pollutant individually. In addition to these anions, water contains cations, the most common of which are calcium (Ca^{2+}), magnesium (Mg^{2+}), sodium (Na^+), and potassium (K^+). To date, only a few studies have looked into the discoloration of BTB using permanganate ions[10,53,54], electrochemical methods[55], and photocatalytic methods[9,56,57]. To the best of our knowledge, there is no kinetic or reaction data on the discoloration of BTB by the SR. In light of these considerations, this study investigates the effect of initial PS and BTB concentrations, temperature, water salts ($Cl^-, HCO_3^-, HPO_4^{2-}, SO_4^{2-}, NO_2^-$ and NO_3^-), and catalytic ions ($Fe^{2+}, Ni^{2+}, Cu^{2+}$, and Ag^+) on the efficiency of BTB discoloration with PS. The steady-state concentrations of the SR were then estimated using both experimental data and numerical simulations. We measured the values of k_6 (SR+ BTB) at temperatures of 40, 50, 60, and 70°C. The obtained results will help

to improve kinetic models, contributing to the refinement and perfection of our understanding of the involved reactions.

2. Materials and Methods

2.1. Products

The following products were utilized: bromothymol blue ($C_{27}H_{28}Br_2O_5S$, 99.5% Biochem Chemopharma), potassium persulfate ($K_2S_2O_8$, 99% Merck), hydrochloric acid (HCl, 37% Honeywell), sulfuric acid (H_2SO_4, 97% Honeywell), iron sulfate heptahydrate ($FeSO_4$ - $7H_2O$, Sigma–Aldrich), nickel sulfate ($NiSO_4$, Biochem Chemopharma), silver nitrate ($AgNO_3$, Biochem Chemopharma), (sodium chloride (NaCl, Honeywell), and sodium bicarbonate ($NaHCO_3$, Honeywell). Diluted solutions of bromothymol blue (BTB) (10 to 30 mg L^{-1}) were prepared from an initial solution of 50 mg L^{-1} to plot the calibration curve and verify that the commercial product followed Beer-Lambert's law. The required quantity of products (PS, salt, transition metals) is added to a flask containing 200 ml of BTB solution, which is heated to the desired temperature with a thermostatic bath.

A double-beam spectrophotometer (DR 2800) was used to conduct kinetic studies on BTB decolorization by PS. The study was conducted at pH 3 (±0.2) and monitored with a Metrohm pH/ionometer model 781 to promote SR formation. The PS and BTB concentrations were chosen to maintain a high PS/BTB ratio and a quasi-stationary state. The UV-Vis spectrophotometer's limitations, including saturation above 30 mg L^{-1} and detection limit below 10 mg L^{-1}, limited our ability to study BTB concentrations.

2.2. Numerical Simulation

Based on the initial experimental conditions ($[PS]_0$, $[BTB]_0$, pH and temperature, we used a numerical simulation model developed in our previous work [58,59] to investigate the reaction between BTB and the dominant SRs (Eq. 6) at pH 3 (SR is dominant). Knowing all the rate constants (k_2-k_5) except k_6 (**Table 2**), the latter is adjusted to ensure that the model matches the experimental results. It should be noted that due to the complexity of the PS reaction mechanism and the extent of the kinetic data, the determined rate constants are subject to significant error.

3. Results and discussion

3.1. Effect of the Initial BTB Concentration

BTB discoloration was performed at four different initial concentrations (0.016, 0.024, 0.032, and 0.048 mM), corresponding to mass concentrations of 10, 15, 20 and 30 mg L^{-1}, respectively. The PS concentration was kept constant at 3.7 mM (1 g L^{-1}) at pH 3 and 60°C. An exponential fit of the experimental data points representing the decrease in BTB concentration allowed the rate constant k_{obs} values of 0.081, 0.059, 0.047 and 0.033 min^{-1} to be calculated. An R^2 value greater than 0.98 indicates that the reaction occurs at a pseudo-first-order rate (**Figure 1**).

The results also show that at lower concentrations, BTB degrades faster and more completely. For example, at 10 mg L^{-}, only 7.82% of the contaminant remains after 30 min, whereas at 30 mg L^{-}, 41.53% remains during the same period. This phenomenon can be explained by the high dye concentration, which results in a low presence of free radicals, reducing the effectiveness of decolorization [60]. These findings are consistent with previous research on the discoloration of crystal violet and E131 dyes by PS [61,62]. These two dyes, like bromothymol blue (BTB), are aromatic hydrocarbons that contain three phenyl rings. To maintain the quasi-steady-state approximation, we chose standard concentrations of PS and BTB at 1 g L^{-1} (3.7 mM) and 10 mg L^{-1} (0.016 mM), respectively. This results in a molar ratio of PS/BTB of 230.

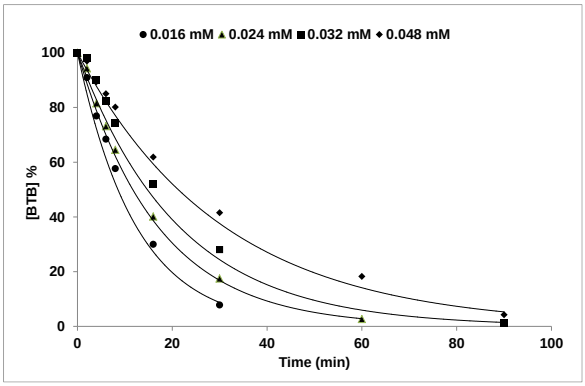

Figure 1. Pseudo first-order kinetics of BTB disappearance by PS (initial conditions: $[PS]_0$ = 3.7 mM, pH = 3 and T = 60°C); [BTB] (%) = $[BTB]_t/[BTB]_0$*100, where $[BTB]_0$ is the concentration at time 0 and $[BTB]_t$ is the concentration at time t.

3.2. Effect of Initial PS Concentration

The effect of PS concentrations (0.037 - 14.8 mM) on the discoloration of BTB (0.016 mM) was investigated at pH 3 and 60°C (**Figure 3**). The values of k_{obs} obtained from the exponential decay of BTB versus time are 0.002, 0.007, 0.040, 0.081, 0.132 and 0.203 min^{-1} at initial PS concentrations of 0.037, 0.185, 1.85, 3.7, 7.4 and 14.8 mM, respectively. The rate constants were found to increase with PS concentration, indicating that the increase could be due to the formation of SR[63]. At low PS concentrations (0.037 mM), degradation is relatively slow, with a BTB removal efficiency of 25%, increasing to 60% at 0.185 mM after 120 min of reaction.

BTB degradation accelerates as the initial PS concentration increases, and complete BTB mineralization occurs in shorter time intervals. For example, at an initial PS concentration of 1.85 mM, BTB decolorization takes 90 min, whereas it only takes 15 min at an initial PS concentration of 14.8 mM. These findings show that the rate of BTB discoloration increased with increasing initial PS concentration. This makes sense because, as the PS concentration rises, more SRs are available to attack the aromatic ring, increasing decolorization efficiency. This observation is consistent with the findings of previous dye studies[13,64].

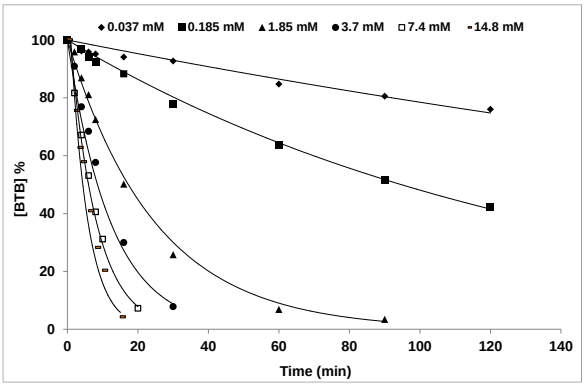

Figure 2. Effect of initial concentration of PS on BTB removal efficiency (initial conditions: $[BTB]_0$ = 0.016 mM, pH = 3 and T = 60°C).

The primary cost-related parameter in any degradation process is oxidant consumption. As a result, in order to treat industrial wastewater economically, the amount of oxidant[42]must be optimized. As a result, we plot the initial PS concentration as a function of BTB half-life values ($t_{1/2}$) in **Figure 3**. The results reveal a nonlinear relationship between $t_{1/2}$ and $[PS]_0$. This result can be explained by the high concentration of PS[13], which causes the following processes to slow down the discoloration mechanism[65]: (a) recombination and annihilation of excess SR (Eq. 5), (b) SR consumption by excess PS (Eq. 3) and (c) the occurrence of an unproductive PS decomposition reaction (with no SR generation).

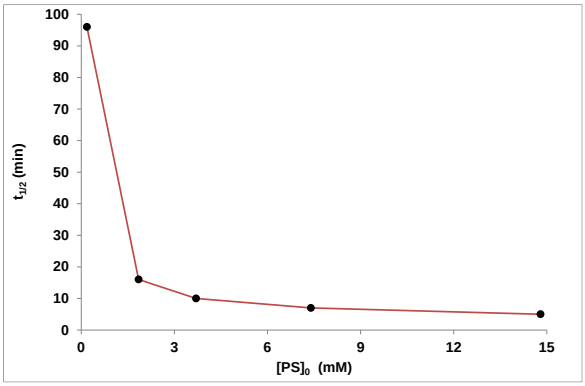

Figure 3. Plot of BTB half-life time ($t_{1/2}$) values as a function of initial PS concentration (initial conditions: $[BTB]_0$ = 0.016 mM, pH = 3 and T = 60°C).

3.3. Effect of Salts

To assess the effect of ions on BTB discoloration, fixed amounts (1 mM) of chloride, sulfate, nitrite, nitrate, hydrogen phosphate, and hydrogen carbonate ions were added to the BTB/PS solution under initial conditions of $[BTB]_0$ = 0.0016 mM, $[PS]_0$ = 3.7 mM, $[Salts]_0$ = 1.0 mM, pH = 3 and T = 60°C. **Figure 4** depicts the evolution of BTB over time in the presence of various salts, demonstrating a gradual decrease. This finding implies that BTB degrades more or less quickly in the experimental solutions than in the control solution (without salt), where the chloride ion is the most effective, and the nitrite ion is the least effective. The other salts, at concentrations of 1 mM, are more or less effective than the control solution. BTB discoloration in the presence of Cl^- is caused by the presence of chloride ions, which react with SR to form chlorine radicals (Eq. 8), increasing the rate of discoloration[66–68].

$$SO_4^{\cdot-} + Cl^- \rightarrow Cl^{\cdot} + SO_4^{2-} \quad (8)$$

This behavior is observed in the degradation of orange acid 7[69] and bisphenol A[70] by heat-activated PS, where the inhibition tendency becomes more pronounced as the Cl^- concentration increases. In addition, during the photocatalytic degradation of BTB[56], adding different concentrations of NaCl resulted in a slight decrease in degradation efficiency as Cl^- concentration increased. This could be due to an excess of chlorine radicals, which react with one another or with the SR and have a negative impact on the degradation process [71]. Chlorine derivatives, including dichloride radical anion ($Cl_2^{\cdot-}$) and chlorine hydroxide radical anion ($ClHO^{\cdot-}$), can affect BTB degradation[72].

$$Cl^{\cdot} + Cl^- \rightarrow Cl_2^{\cdot-} \quad (9)$$

Initially, at a high reaction rate constant of nitrite with SR equal to 8.8×10^8 M^{-1} s^{-1}[73], the nitrite ion competes with the organic pollutants for SR (Eq. 10), leading to the formation of nitrogen dioxide radicals ($NO_2^{\cdot-}$) [74], and a decrease in SR concentration.

$$SO_4^{\cdot-} + NO_2^- \rightarrow NO_2^{\cdot-} + SO_4^{2-} \quad (10)$$

For example, the presence of nitrite ions reduced the SR degradation efficiency of phenol[71] and tetrabromobisphenol S[75]. Nitrogen dioxide played a significant role in the degradation of aniline by the SR, accounting for approximately 42.3% of the transformation. Finally, the degradation efficiency is determined by the rate at which the radicals react with the organic pollutant. If the rate constant for nitrite ion is higher than that of SR, the degradation process is accelerated. A lower rate constant for NO_2^- slows the degradation process.

Bicarbonate (HCO_3^-), monohydrogen phosphate (HPO_4^{2-}), and nitrate (NO_3^-) ions react with SRs to produce bicarbonate, monohydrogen phosphate and nitrate radical anions at rates of 9.1×10^6, 1.6×10^6 and 2.1×10^6 M^{-1} s^{-1}[73,76], respectively. The rate constants are lower than those for nitrite ion, resulting in less

pronounced SR scavenging. Furthermore, these radicals are less reactive towards organic molecules, with effects ranging from negligible to negative. For example, the presence of these ions can have a negative impact on the degradation of orange G by PS[77]. Regarding the effect of the sulfate ion, adding an amount equal to that present in the solution (1 mM) and continuously producing this ion during the reaction (Eqs. 3 and 4) had little effect on BTB degradation when compared to the control solution. According to other studies on the degradation of trichloroethane[78] and benzotriazole[52] by PS, the effect of this ion on pollutant oxidation is minimal. This is because there is no reaction between the ion and the SR, so it is possible that the literature has not highlighted a significant reaction between sulfate ion and SR[39,79], as their reaction may be negligible or insignificant in comparison to other reactions in the PS degradation process.

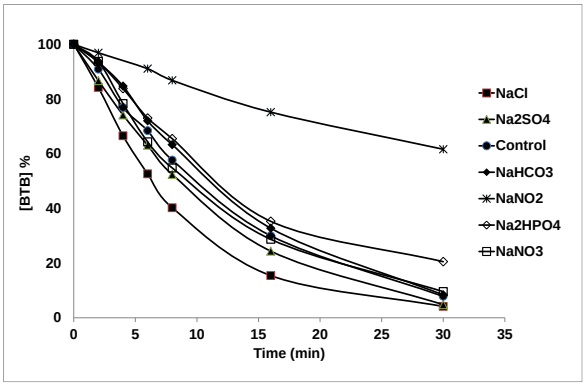

Figure 4: Effects of salts on the discoloration of BTB (initial conditions: $[BTB]_0$ = 0.0016 mM, $[PS]_0$ = 3.7 mM, $[Salts]_0$ = 1.0 mM, pH = 3 and T = 60°C).

The variation in ionic strength (**Table 1**) indicates a lack of proportionality between ionic strength and BTB discoloration efficiency (k_{Obs}). Several studies have found that ionic strength influences the degradation of organic pollutants by PS[80,81]. The small variation in ionic strength (14 ± 1.6 mM) may explain the lack of a significant correlation between ionic strength and BTB decolorization efficiency (k_{obs}). However, injecting the same concentrations of KCl and NaCl (1 mM) into the BTB solution (**Figure 5**) does not produce the same discoloration kinetics (0.061 and 0.109 min^{-1}, respectively). Despite having the same ionic strength of 0.0136 M, monocations have distinct effects on BTB decolorization. The same result is seen in the degradation of E110 by PS[82]. This phenomenon can be explained by the size difference between sodium and potassium atoms, which affects their ionic character in solution[83].

Table 1. Ionic strength variations in BTB discoloration at different types of salts (initial conditions: $[BTB]_0$ = 0.0016 mM, $[PS]_0$ = 3.7 mM, $[Salts]_0$ = 1.0 mM, pH = 3 and T = 60°C).

Solution	Ionic strengths mM	k_{Obs} (min^{-1})
BTB/PS/H_2SO4	12.6	0.0812
BTB/PS/H_2SO4/$NaHCO_3$	13.6	0.0774
BTB/PS/H_2SO4/NaCl	13.6	0.109
BTB/PS/H_2SO4/KCl	13.6	0.061
BTB/PS/H_2SO_4/Na_2SO_4	15.6	0.0965
BTB/PS/H_2SO_4/Na_2HPO4	15.6	0.0551
BTB/PS/H_2SO_4/$NaNO_2$	13.6	0.0165
BTB/PS/H_2SO_4/$NaNO_3$	13.6	0.0165

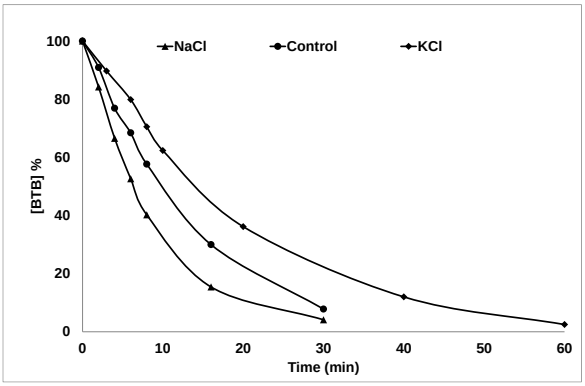

Figure 5. Effects of salts on the discoloration of BTB (initial conditions: $[BTB]_0$ = 0.0016 mM, $[PS]_0$ = 3.7 mM, $[Salts]_0$ = 1.0 mM, pH = 3 and T = 60°C).

3.4. Effect of Transition Metals

Figure 6 compares the effects of various PS activation methods by transition metals (Fe^{2+}, Ni^{2+}, Cu^{2+}, and Ag^{+}) on BTB discoloration. The experiments began with the following initial concentrations of BTB, PS, and transition metals: 0.016, 3.7, and 0.8 mM, respectively, and an initial pH of 3. When silver was added to BTB, it discolored quickly, whereas iron caused it to discolor slowly. The presence of nickel and copper in the system did not cause BTB discoloration. In fact, it has been reported that silver ions are one of the most effective catalysts among homogeneous metal ions and oxides[84], while iron is less effective but widely used due to its environmental benefits[48] and role in the Fenton effect process[60]. Many studies have found that nickel and copper are ineffective activators of PS[85,86]. The experiment in which no metal was present when PS was mixed with BTB at room temperature resulted in no discoloration of BTB. This is due to the limited generation of SRs in this temperature range, resulting in a slower discoloration rate and, as a result, a discoloration efficiency that lasts several tens of days[87,88].

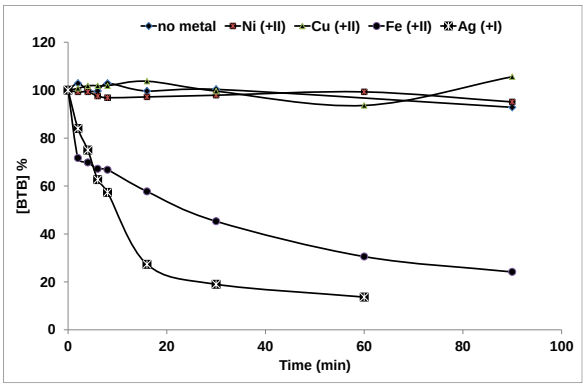

Figure 6. Effects of transition metals on the discoloration of BTB: ($[BTB]_0$ = 0.0016 mM, $[PS]_0$ = 3.7 mM, pH = 3 and T = 25°C).

3.5. Effect of Iron (II) Concentrations

The Fe (II)-activated PS process has been applied to wastewater treatment, particularly for in situ chemical oxidation with SRs[89]. However, the presence of ferric ions may alter the discoloration mechanism of BTB by reacting with SRs (Eq. 11). To assess the oxidation of BTB by SRs in the presence of Fe (II) ions, we discolored BTB at concentrations of 0.2 mM and 0.8 mM Fe. In addition, we added 0.8 mM Fe (II) to the solution four times over 90 min (**Figure 7**). We found that increasing the amount of iron added (from 0.2 to 0.8 mM) improved BTB discoloration slightly, from 70% at 0.2 mM to 75% at 0.8 mM. However, when we gradually increased the iron concentration from 0.2 mM to 0.8 mM, the final BTB removal efficiency reached 86%. As a result, higher Fe (II) concentrations accelerated PS activation to SR (Eq. 10), but Fe (II) was also oxidized to Fe (III) by SR, lowering its concentration (Eq. 11).

$$SO_4^{\cdot -} + Fe^{2+} \rightarrow Fe^{3+} + SO_4^{2-} \quad (11)$$

A gradual addition of Fe (II) is required to facilitate PS oxidation into SRs[24,25,90]. When using an iron anode for electrochemical Fe (II) supply, the generation of Fe (II) can be controlled by adjusting the current [89,91]. Therefore, this electrochemical method outperforms others in terms of PS activation.

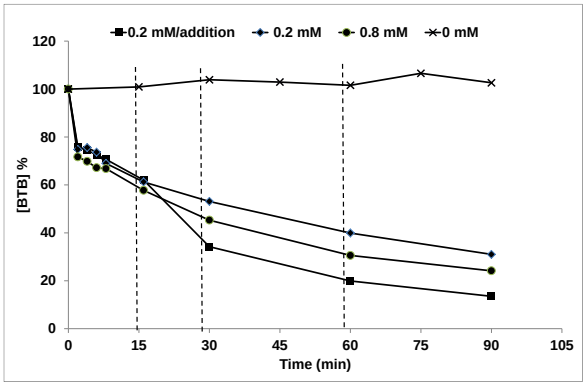

Figure 7. Influence of Fe (II) concentration on the removal of BTB: ($[BTB]_0$ = 0.0016 mM, $[PS]_0$ = 3.7 mM, pH = 3 and T = 25°C). For the successive addition of Iron (0.2 mM/addition), each vertical line indicates the addition of 0.0002 mM.

3.6. Effect of Temperature

The impact of temperature on BTB discoloration was studied at four different heating temperatures (40, 50, 60, and 70°C). In all experiments, the initial BTB concentration was set to 0.0016 mM and predicted during discoloration using numerical simulation. BTB degradation (**Figure 8**) follows first-order kinetics, with the rate increasing with temperature. At 70°C, degradation is nearly complete in 16 min, whereas at 60°C, it is faster but less noticeable, with 7.82% of the product remaining after 30 min. At 50°C and 40°C, degradation is much slower, with 52% and 36.50% of the product remaining after 30 and 270 min, respectively; higher temperatures promote faster degradation. Thus, the positive effect of increased heating on BTB disappearance, which shortens the time required for decolorization, is clearly visible. This can be explained by the increased generation of SRs proportional to temperature, which causes the fission of the O-O bond in PS[13], resulting in a faster rate of BTB decomposition. In addition, the simulation model enabled us to determine the reaction rate of SR with BTB using the initial experimental conditions ($[PS]_0$, $[BTB]_0$, pH and temperature) and the reaction rate constants (k_2 to k_5) (**Table 2**).

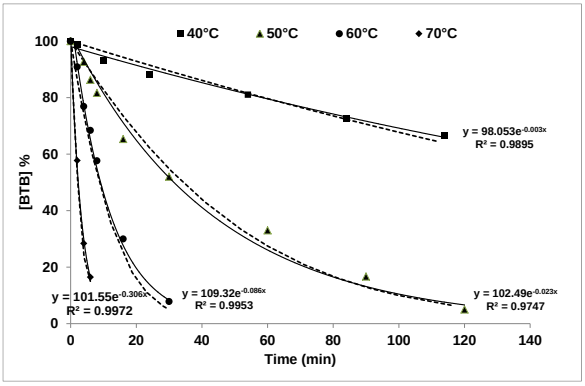

Figure 8. Plot of BTB discoloration at different temperatures ($[BTB]_0$ = 0.0016 mM, $[PS]_0$ = 3.7 mM, pH = 3). The solid and dashed lines correspond to the simulation fit and exponential fit of each experience, respectively.

Table 2. Rate constants for BTB discoloration.

Chemical reactions	Rate constants					
	40°C	50°C	60°C	70°C	Units	References
Eq. (2)	3.36	19.4	59.4	222	$\times 10^{-7}$ [s^{-1}]	[92]
Eq. (3)	6.1	6.1	6.1	6.1	$\times 10^{5}$ [M^{-1} s^{-1}]	[93]
Eq. (4) *	7.4	8.3	9.2	10.2	$\times 10^{2}$ [s^{-1}]	[19]
Eq. (5)	4.8	4.8	4.8	4.8	$\times 10^{8}$ [M^{-1} s^{-1}]	[94]

**The indicated rate constant is equal to $k_4 \times [H_2O]$.*

Table 3 shows that the values of k_6 at 40, 50, 60 and 70°C: $(1.1 \pm 0.55) \times 10^8$, $((1.5 \pm 0.77) \times 10^8$, $(1.9 \pm 0.95) \times 10^8$ and $(2.2 \pm 1.1) \times 10^8$ M^{-1} s^{-1}, respectively, as a result of the numerical simulation. The reaction rate only doubles at activation energies of about 50 kJ mol^{-1} for temperatures in the 10 °C range, according to several studies[40,64,95]. The calculated k_6 values reveal that the rate constants at two successive temperatures differ by less than a factor of two. That being the case, the activation energy that we shall ascertain in due course cannot exceed 50 kJ mol^{-1}. Additionally, the second-order rate constants for the reactions involving SR and organic compounds in aqueous solutions range from 10^5 to 10^{10} M^{-1} s^{-1}[96]. The presence of substituents that donate electrons can cause these values to rise, while the presence of substituents that withdraw electrons can cause them to fall[96]. For example, Brilliant Green shares similarities with BTB, as both have three aromatic rings and contain two $-N(Et)_2$ groups, which are electron-donating. Compared to BTB, which has a combination of electron-donating and electron-withdrawing groups[6], brilliant green exhibits a higher rate constant[97] of 2.21×10^9 M^{-1} s^{-1} when reacting with SRs at room temperature.

Table 3. Obtained values of $[SO_4^{\bullet-}]_{ss}$ and k_6 based on numerical simulation.

T [°C]	$[PS]_0$ [mM]	$[BTB]_0$ [mM]	k_{obs} 10^{-5} [s^{-1}]	$[SO_4^{\bullet-}]_{ss}$ (10^{-12} [M])	k_6 (10^8 [M^{-1} s^{-1}])
40	3.7	0.0016	0.00006	0.5	1.1 ± 0.55
50	3.7	0.0016	0.0004	2.57	1.55 ± 0.77
60	3.7	0.0016	0.0014	6.78	1.9 ± 0.95*
70	3.7	0.0016	0.0045	22.3	2.2 ± 1.1

*All errors represent ± 2σ (measurement errors), *with errors calculated from experiments carried out at 60°C*

The steady-state concentrations of SRs obtained in this study are in good agreement with those reported by other researchers. The steady-state concentrations of SRs at room temperature for 15 pharmaceutical products with rate constants ranging from 10^8 and 10^9 M^{-1} s^{-1} and a PS concentration of 1 mM were calculated by Lian et al. [16] to be $(2.21 \pm 0.06) \times 10^{-13}$ M. Several other steady-state concentrations of SR, similar to the value obtained in our study, have been determined in previous investigations[19,98]. The obtained values of the reaction rate constant between SR and BTB (k_6) were used to calculate the values of the kinetic activation parameters: activation energy (E_a), enthalpy ($\Delta H^{\neq}$), entropy ($\Delta S^{\neq}$), and Gibbs free energy ($\Delta G^{\neq}$). Using the Arrhenius and Eyring equations (Eqs. 12, 13, and 14) [61,90], and by plotting $\ln(k_6)$ and $\ln(k_6/T)$ vs 1/T, respectively (**Figure 9**).

$$\ln(k_6) = \ln A - \frac{E_a}{RT} \quad (12)$$

A = frequency factor

E_a = Activation energy (kJ mol^{-1})

R = Gas constant (J.mol^{-1} K^{-1})

T = Absolute temperature (K)

$$\ln\left(\frac{k_6}{T}\right) = \ln\left(\frac{k_B}{h}\right) + \frac{\Delta S^{\neq}}{R} - \frac{\Delta H^{\neq}}{RT} \quad (13)$$

- k_B is the Boltzmann constant (1.38 × 10^{-23} J K^{-1}),
- h is Planck's constant (6.626 × 10^{-34} J s),
- $\Delta H^{\neq}$ and $\Delta S^{\neq}$ are the enthalpy and entropy of activation, respectively.

The free activation energy ($\Delta G^{\neq}_{298}$) was calculated at a temperature of 298.15 K using Eq. (13):

$$\Delta G^{\neq}_{298} = \Delta H^{\neq} - T\Delta S^{\neq} \quad (14)$$

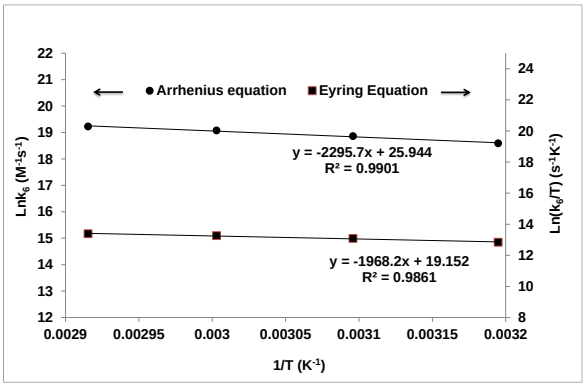

Figure 9. Arrhenius plot for BTB discoloration ([BTB]$_0$ = 0.0016 mM, [PS]$_0$ = 3.7 mM, pH = 3 and T = 40, 50, 60 and 70°C).

The activation thermodynamic parameters (**Table 4**) of the decolorization BTB by PS were calculated using the data from **Figure 9**. When heated, PS[61] discolors crystal violet, a triphenylmethane dye similar to BTB, with thermodynamic parameters similar to BTB: 28.9 kJ mol^{-1} for activation energy, 26.4 kJ mol^{-1} for enthalpy, - 0.235 kJ mol^{-1} K^{-1} for entropy, and 96.4 kJ mol^{-1} for free energy of activation. At pH 3, Maamar et al. [55]investigated BTB discoloration using the electro-Fenton process and found that the reaction between BTB and hydroxyl radicals had a low activation energy value of 9.66 kJ mol^{-1}. Furthermore, rhodamine B[90] and acid blue 92[13] both show low activation energies of 36.5 kJ mol^{-1} and 17.38 kJ mol^{-1}, respectively, when discolored by heated PS in the case of molecules with three benzene rings.

Table 4. Activation thermodynamic parameters of the decolorization BTB by PS ([BTB]$_0$ = 0.0016 mM, [PS]$_0$ = 3.7 mM, pH = 3 and T = 40, 50, 60 and 70°C)

E_a (kJ mol^{-1})	$\Delta H^{\neq}$ (kJ mol^{-1})	$\Delta S^{\neq}$ (kJ mol^{-1} K^{-1})	$\Delta G^{\neq}_{298}$ (kJ mol^{-1})
19.8	16.36	- 0.038	27.78

3.7. UV–VIS Spectrum of BTB and Discoloration Mechanism

To study the evolution of the BTB molecule during PS oxidation, we tracked its UV-VIS spectrum. This spectrum contains three distinct bands: the most intense at 432 nm, which is responsible for the yellow color, and two bands at 330 nm and 277 nm in the UV region due to unsaturation in the aromatic ring. **Figure 10** shows the discoloration of the BTB dye caused by oxidation with heated activated PS. After 180 min, the absorption peak at λ = 433 nm gradually decreases and disappears. This is followed by the formation of intermediates that absorb at around 320 nm and are then oxidized by the reaction medium.

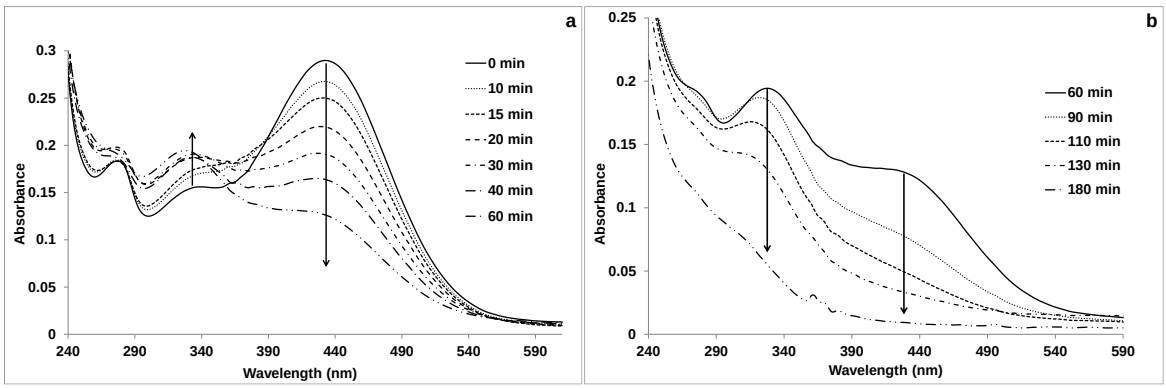

Figure 10. UV–Vis spectrum evolution of BTB through PS oxidation: a) from 0 to 60 min, and b) from 60 to 180 min.

The absorbance at 330 and 277 nm slowly increases for up to 60 min (**Figure 10a**), then gradually decreases until both peaks disappear (**Figure 10b**). Numerous researchers[99,100]have suggested that the initial step in the oxidation of triphenylmethane molecules involves an attack on the central carbon atom. We propose that a similar mechanism applies to BTB. This action disrupts the extensive conjugation of the chromophore system, resulting in rapid depletion of the visible band. The decrease in the UV-visible spectrum is likely due to the complete mineralization of BTB[90]. A new peak appears at 330 nm without a hypochromic shift, indicating the cleavage of the entire conjugated chromophore structure of BTB and the formation of an intermediate compound, possibly aromatic intermediates[101,102].

There is also a gradual increase in absorbance at 330 and 277 nm, indicating the degradation of the aromatic structure[62]. SRs can react with organic molecules via one of three oxidation pathways: electron transfer, double bond addition, or hydrogen abstraction[96]. In general, the action of SRs on organic compounds leads to hydroxylation. SRs react with water to produce hydroxyl radicals (Eq. 4), which then react with aromatic rings to form hydroxyl adducts[93,103]. Additionally, SRs could directly attack the aromatic ring and form hydroxyl adducts[93,104], or both processes may occur simultaneously[105]. According to the present results and the literature[93,96,103,106], BTB oxidation can occur via the following mechanisms:

1) formation of intermediates potentially involving c-demethylation pathways,
2) creation of fully dealkylated products,
3) removal of an aryl ring,
4) hydroxylation of the aryl and sulfonylated benzene rings,
5) substitution of hydroxyl groups within the sulfonate groups and sulfate adducts,
6) symmetric and asymmetric cleavage processes.

Thus, we propose a reaction mechanism that outlines potential BTB degradation pathways by SRs (**Figure 11**).

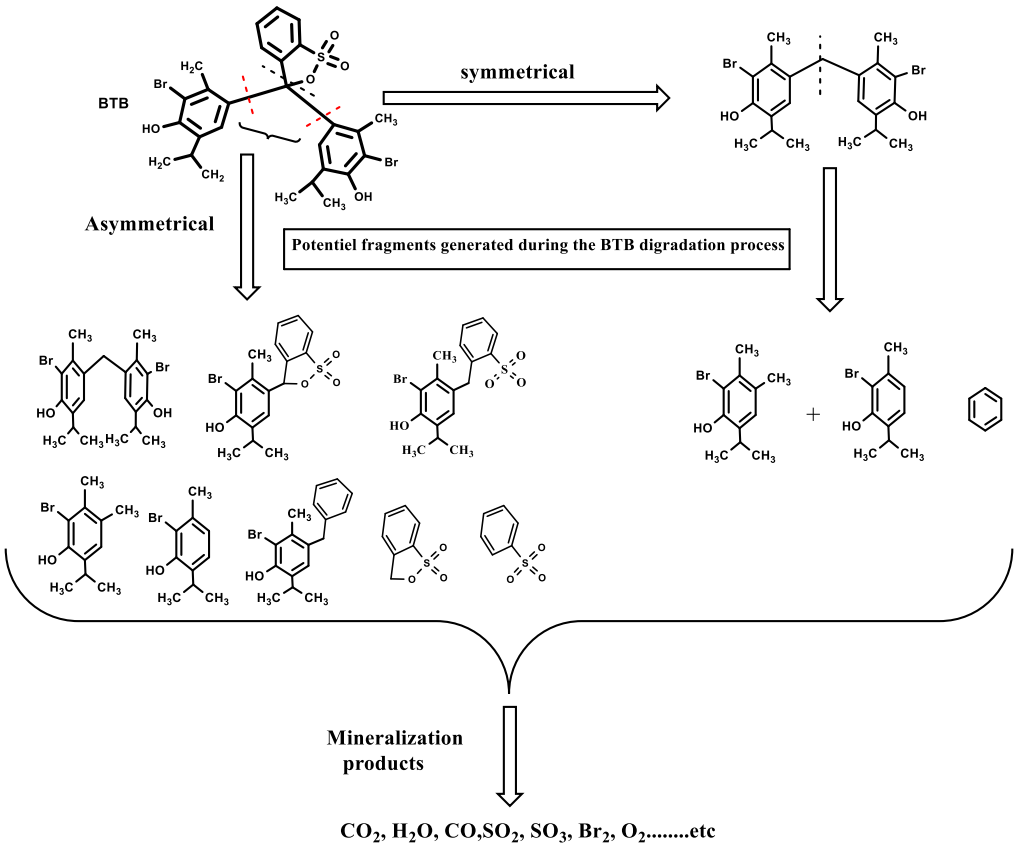

Figure 11. Possible pathways for the degradation of BTB by SR anions

4. Conclusion

This study investigated the discoloration of bromothymol blue in an aqueous solution using thermally activated PS at pH 3. The effects of various variables, such as dye concentration, peroxydisulfate dosages, matrix water, and temperature, were investigated. The optimal operating conditions were set to $[BTB]_0$ = 0.0016 mM, $[PS]_0$ = 3.7 mM, pH = 3 and T= 60°C. In the given conditions, more than 90% of the decolorization efficiency was achieved in 30 min. The anions and cations used in this study demonstrated varying efficiencies in BTB degradation. The numerical simulation allowed us to predict the values of the reaction rate constant between SR and BTB at various temperatures, which increase as the reaction temperature rises. The calculated k_6 values show that the rate constants at two successive temperatures differ by less than a factor of two, which is consistent with the activation energy of 19.8 kJ mol^{-1}. Finally, a tentative mechanism for BTB degradation by SR was proposed, in which the destruction of aromatic ring structures occurs concurrently with BTB discoloration.

Author contributions

Conceptualization, NL; methodology, NL and MD; validation, NL and MD; investigation, MB and NL; resources, MB and NL; data curation, AT and SB; writing—original draft preparation, NL; writing—review and editing, MD; visualization, NL, MD and MB; supervision, MD. All authors have read and agreed to the published version of the manuscript.

Conflict of interest

No conflict of interest exists.

References

1. Maheshwari K, Agrawal M, Gupta AB. Dye pollution in water and wastewater. In: novel materials for dye-containing wastewater treatment. (Muthu SS, Khadir A. eds). Sustainable Textiles: Production, Processing, Manufacturing & Chemistry Springer Singapore: Singapore; 2021; pp. 1–25; doi: 10.1007/978-981-16-2892-4_1.
2. Li N, Wu S, Dai H, et al. Thermal activation of persulfates for organic wastewater purification: heating modes, mechanism and influencing factors. Chem Eng J 2022;450:137976; doi: 10.1016/j.cej.2022.137976.
3. Wang J, Wang S. Removal of pharmaceuticals and personal care products (ppcps) from wastewater: A review. J Environ Manage 2016;182:620–640; doi: 10.1016/j.jenvman.2016.07.049.
4. Pavithra KG, P. SK, V. J, et al. Removal of colorants from wastewater: a review on sources and treatment strategies. J Ind Eng Chem 2019;75:1–19; doi: 10.1016/j.jiec.2019.02.011.
5. Giasuddin ABM, Kanel SR, Choi H. Adsorption of humic acid onto nanoscale zerovalent iron and its effect on arsenic removal. Environ Sci Technol 2007;41:2022–2027; doi: 10.1021/es0616534.
6. De Meyer T, Steyaert I, Hemelsoet K, et al. Halochromic properties of sulfonphthaleine dyes in a textile environment: the influence of substituents. Dyes Pigments 2016;124:249–257; doi: 10.1016/j.dyepig.2015.09.007.
7. Thomas O, Brogat M. Organic Constituents. In: UV-Visible spectrophotometry of waters and soils Elsevier; 2022; pp. 95–160; doi: 10.1016/B978-0-323-90994-5.00006-X.
8. Van der Schueren L, De Clerck K. Textile materials with a pH-sensitive function. Sariişik M. ed. Int J Cloth Sci Technol 2011;23:269–274; doi: 10.1108/09556221111136539.
9. Soukeur A, Kaci MM, Omeiri S, et al. Photocatalytic degradation of bromothymol blue over MgFe2O4 under sunlight exposure. Opt Mater 2023;142:114108; doi: 10.1016/j.optmat.2023.114108.
10. Ibrahim SM, Al-Hossainy AF. Synthesis, structural characterization, DFT, kinetics and mechanism of oxidation of bromothymol blue: application to textile industrial wastewater treatment. Chem Pap 2021;75:297–309; doi: 10.1007/s11696-020-01299-8.
11. Matzek LW, Carter KE. Activated persulfate for organic chemical degradation: A review. Chemosphere 2016;151:178–188; doi: 10.1016/j.chemosphere.2016.02.055.
12. Ma J, Li H, Chi L, et al. Changes in activation energy and kinetics of heat-activated persulfate oxidation of phenol in response to changes in pH and temperature. Chemosphere 2017;189:86–93; doi: 10.1016/j.chemosphere.2017.09.051.
13. Ahmadi S, Igwegbe CA, Rahdar S. The application of thermally activated persulfate for degradation of acid blue 92 in aqueous solution. Int J Ind Chem 2019;10:249–260; doi: 10.1007/s40090-019-0188-1.
14. Yang B, Luo Q, Li Q, et al. Selective oxidation and direct decolorization of cationic dyes by persulfate without activation. Water Sci Technol 2021;83(11):2744–2752; doi: 10.2166/wst.2021.177.
15. Giannakis S, Lin K-YA, Ghanbari F. A review of the recent advances on the treatment of industrial wastewaters by sulfate radical-based advanced oxidation processes (SR-AOPs). Chem Eng J 2021;406:127083; doi: 10.1016/j.cej.2020.127083.
16. Lian L, Yao B, Hou S, et al. Kinetic study of hydroxyl and sulfate radical-mediated oxidation of pharmaceuticals in wastewater effluents. Environ Sci Technol 2017;51(5):2954–2962; doi: 10.1021/acs.est.6b05536.
17. Furman OS, Teel AL, Watts RJ. Mechanism of base activation of persulfate. Environ Sci Technol 2010;44:6423–6428; doi: 10.1021/es1013714.
18. Liang C-J, Huang S-C. Kinetic model for sulfate/hydroxyl radical oxidation of methylene blue in a thermally-activated persulfate system at various pH and temperatures. Sustain Env Res 2012;199–208.
19. Mora VC, Rosso JA, Carrillo Le Roux G, et al. Thermally activated peroxydisulfate in the presence of additives: A clean method for the degradation of pollutants. Chemosphere 2009;75:1405–1409; doi: 10.1016/j.chemosphere.2009.02.038.
20. El-Bestawy EA, Gaber M, Shokry H, et al. Effective degradation of atrazine by spinach-derived biochar via persulfate activation system: Process optimization, mechanism, degradation pathway and application in real wastewater. Environ Res 2023;229:115987; doi: 10.1016/j.envres.2023.115987.
21. Habibi M, Habibi-Yangjeh A, Pouran SR, et al. Visible-light-triggered persulfate activation by CuCo2S4 modified ZnO photocatalyst for degradation of tetracycline hydrochloride. Colloids Surf Physicochem Eng Asp 2022;642:128640; doi: 10.1016/j.colsurfa.2022.128640.
22. Li N, Wang Y, Cheng X, et al. Influences and mechanisms of phosphate ions onto persulfate activation and organic degradation in water treatment: A review. Water Res 2022;222:118896; doi: 10.1016/j.watres.2022.118896.
23. Bing W, Wei W. Degradation phenol wastewater by heating activated persulfate. Int J Environ Monit Anal 2019;7:14; doi: 10.11648/j.ijema.20190701.12.

24. Wang Z, Qiu W, Pang S, et al. Relative contribution of ferryl ion species (Fe(IV)) and sulfate radical formed in nanoscale zero valent iron activated peroxydisulfate and peroxymonosulfate processes. Water Res 2020;172:115504; doi: 10.1016/j.watres.2020.115504.
25. Dong H, He Q, Zeng G, et al. Degradation of trichloroethene by nanoscale zero-valent iron (nZVI) and nZVI activated persulfate in the absence and presence of EDTA. Chem Eng J 2017;316:410–418; doi: 10.1016/j.cej.2017.01.118.
26. Hou S, Ling L, Shang C, et al. Degradation kinetics and pathways of haloacetonitriles by the UV/persulfate process. Chem Eng J 2017;320:478–484; doi: 10.1016/j.cej.2017.03.042.
27. Ghauch A, Baalbaki A, Amasha M, et al. Contribution of persulfate in UV-254 nm activated systems for complete degradation of chloramphenicol antibiotic in water. Chem Eng J 2017;317:1012–1025; doi: 10.1016/j.cej.2017.02.133.
28. Dhaka S, Kumar R, Khan MA, et al. Aqueous phase degradation of methyl paraben using UV-activated persulfate method. Chem Eng J 2017;321:11–19; doi: 10.1016/j.cej.2017.03.085.
29. Miao D, Zhao S, Zhu K, et al. Activation of persulfate and removal of ethyl-parathion from soil: Effect of microwave irradiation. Chemosphere 2020;253:126679; doi: 10.1016/j.chemosphere.2020.126679.
30. Gao Y, Gao N, Wang W, et al. Ultrasound-assisted heterogeneous activation of persulfate by nano zero-valent iron (nZVI) for the propranolol degradation in water. Ultrason Sonochem 2018;49:33–40; doi: 10.1016/j.ultsonch.2018.07.001.
31. Matzek LW, Tipton MJ, Farmer AT, et al. Understanding electrochemically activated persulfate and its application to ciprofloxacin abatement. Environ Sci Technol 2018;52:5875–5883; doi: 10.1021/acs.est.8b00015.
32. Santos A, Fernandez J, Rodriguez S, et al. Abatement of chlorinated compounds in groundwater contaminated by HCH wastes using ISCO with alkali activated persulfate. Sci Total Environ 2018;615:1070–1077; doi: 10.1016/j.scitotenv.2017.09.224.
33. Koltsakidou A, Antonopoulou M, Evgenidou E, et al. A comparative study on the photo-catalytic degradation of Cytarabine anticancer drug under Fe3+/H2O2, Fe3+/S2O82−, and [Fe(C2O4)3]3−/H2O2 processes. Kinetics, identification, and in silico toxicity assessment of generated transformation products. Environ Sci Pollut Res 2019;26:7772–7784; doi: 10.1007/s11356-018-4019-2.
34. Arvaniti OS, Ioannidi AA, Mantzavinos D, et al. Heat-activated persulfate for the degradation of micropollutants in water: A comprehensive review and future perspectives. J Environ Manage 2022;318:115568; doi: 10.1016/j.jenvman.2022.115568.
35. Sipilä K. Cogeneration, biomass, waste to energy and industrial waste heat for district heating. In: Advanced District Heating and Cooling (DHC) Systems Elsevier; 2016; pp. 45–73; doi: 10.1016/B978-1-78242-374-4.00003-3.
36. Sakulthaew C, Chokejaroenrat C, Satapanajaru T, et al. Removal of 17β-estradiol using persulfate synergistically activated using heat and ultraviolet light. Water Air Soil Pollut 2020;231(5):247; doi: 10.1007/s11270-020-04571-5.
37. Liu X, Wang Z, Liang H, et al. Solar-Driven soil remediation along with the generation of water vapor and electricity. Nanomaterials 2022;12(11):1800; doi: 10.3390/nano12111800.
38. Mekhilef S, Faramarzi SZ, Saidur R, et al. The application of solar technologies for sustainable development of agricultural sector. Renew Sustain Energy Rev 2013;18:583–594; doi: 10.1016/j.rser.2012.10.049.
39. Wacławek S, Lutze HV, Grübel K, et al. Chemistry of persulfates in water and wastewater treatment: A review. Chem Eng J 2017;330:44–62; doi: 10.1016/j.cej.2017.07.132.
40. House DA. kinetics and mechanism of oxidations by peroxydisulfate. Chem Rev 1962;62:185–203; doi: 10.1021/cr60217a001.
41. Chen W-S, Huang C-P. Mineralization of aniline in aqueous solution by electrochemical activation of persulfate. Chemosphere 2015;125:175–181; doi: 10.1016/j.chemosphere.2014.12.053.
42. Shuchi SB, Suhan MdBK, Humayun SB, et al. Heat-activated potassium persulfate treatment of sudan black b dye: Degradation kinetic and thermodynamic studies. J Water Process Eng 2021;39:101690; doi: 10.1016/j.jwpe.2020.101690.
43. Sonawane S, Rayaroth MP, Landge VK, et al. Thermally activated persulfate-based advanced oxidation processes — recent progress and challenges in mineralization of persistent organic chemicals: a review. Curr Opin Chem Eng 2022;37:100839; doi: 10.1016/j.coche.2022.100839.
44. Zhou T, Du J, Wang Z, et al. Degradation of sulfamethoxazole by MnO2/heat-activated persulfate: Kinetics, synergistic effect and reaction mechanism. Chem Eng J Adv 2022;9:100200; doi: 10.1016/j.ceja.2021.100200.
45. Liu Y, Wang S, Wu Y, et al. Degradation of ibuprofen by thermally activated persulfate in soil systems. Chem Eng J 2019;356:799–810; doi: 10.1016/j.cej.2018.09.002.

46. Anipsitakis GP, Dionysiou DD. Radical generation by the interaction of transition metals with common oxidants. Environ Sci Technol 2004;38:3705–3712; doi: 10.1021/es035121o.
47. Anipsitakis GP, Dionysiou DD. Transition metal/UV-based advanced oxidation technologies for water decontamination. Appl Catal B Environ 2004;54(3):155–163; doi: 10.1016/j.apcatb.2004.05.025.
48. Wei L, Xia X, Zhu F, et al. Dewatering efficiency of sewage sludge during Fe2+-activated persulfate oxidation: Effect of hydrophobic/hydrophilic properties of sludge EPS. Water Res 2020;181:115903; doi: 10.1016/j.watres.2020.115903.
49. Pignatello JJ, Oliveros E, MacKay A. Advanced oxidation processes for organic contaminant destruction based on the fenton reaction and related chemistry. Crit Rev Environ Sci Technol 2006;36(1):1–84; doi: 10.1080/10643380500326564.
50. Lu J, Wu J, Ji Y, et al. Transformation of bromide in thermo activated persulfate oxidation processes. Water Res 2015;78:1–8; doi: 10.1016/j.watres.2015.03.028.
51. Chiron S, Minero C, Vione D. Occurrence of 2,4-dichlorophenol and of 2,4-dichloro-6-nitrophenol in the rhône river delta (southern france). Environ Sci Technol 2007;41(9):3127–3133; doi: 10.1021/es0626638.
52. Ma J, Ding Y, Chi L, et al. Degradation of benzotriazole by sulfate radical-based advanced oxidation process. Environ Technol 2021;42(2):238–247; doi: 10.1080/09593330.2019.1625959.
53. Ibrahim SM, Al-Hossainy AF. Kinetics and mechanism of oxidation of bromothymol blue by permanganate ion in acidic medium: Application to textile industrial wastewater treatment. J Mol Liq 2020;318:114041; doi: 10.1016/j.molliq.2020.114041.
54. Al-Hossainy AF, Ibrahim SM. Oxidation process and kinetics of bromothymol blue by alkaline permanganate. Int J Chem Kinet 2021;53:675–684; doi: 10.1002/kin.21473.
55. Maamar M, Naimi I, Mkadem Y, et al. Electrochemical oxidation of bromothymol blue: application to textile industrial wastewater treatment. J Adv Oxid Technol 2015;18(1); doi: 10.1515/jaots-2015-0113.
56. Bouanimba N, Laid N, Zouaghi R, et al. A comparative study of the activity of tio2 degussa p25 and millennium pcs in the photocatalytic degradation of bromothymol blue. Int J Chem React Eng 2018;16; doi: 10.1515/ijcre-2017-0014.
57. Machado PR, Soeira TVR, Pagan FDS, et al. Synergistic bromothymol blue dye degradation with hydrodynamic cavitation and hydrogen peroxide (HC-H2O2). Ambiente E Agua - Interdiscip J Appl Sci 2020;15:1; doi: 10.4136/ambi-agua.2518.
58. Djehiche M, Tomas A, Fittschen C, et al. First direct detection of hono in the reaction of methylnitrite (CH_3ONO) with OH Radicals. Environ Sci Technol 2011;45:608–614; doi: 10.1021/es103076e.
59. Djehiche M, Tomas A, Fittschen C, et al. First cavity ring-down spectroscopy ho $_2$ measurements in a large photoreactor. Z Für Phys Chem 2011;225:938–992; doi: 10.1524/zpch.2011.0143.
60. Sun S-P, Li C-J, Sun J-H, et al. Decolorization of an azo dye orange g in aqueous solution by Fenton oxidation process: Effect of system parameters and kinetic study. J Hazard Mater 2009;161(2–3):1052–1057; doi: 10.1016/j.jhazmat.2008.04.080.
61. Fayoumi LMA, Ezzedine MA, Akel HH, et al. Kinetic study of the degradation of crystal violet by K2S2O8. Comparison with Malachite Green: Port Electrochimica Acta 2012;30(2):121–133; doi: 10.4152/pea.201202121.
62. Naser Elddine HA, Damaj ZK, Yazbeck OA, et al. Kinetic study of the discoloration of the food colorant E131 by K2S2O8 and KIO3: Port Electrochimica Acta 2015;33(5):275–288; doi: 10.4152/pea.201505275.
63. Thabet M, El-Zomrawy AA. Degradation of acid red 17 dye with ammonium persulphate in acidic solution using photoelectrocatalytic methods. Arab J Chem 2016;9:S204–S208; doi: 10.1016/j.arabjc.2011.03.001.
64. Ahmadi M, Behin J, Mahnam AR. Kinetics and thermodynamics of peroxydisulfate oxidation of reactive yellow 84. J Saudi Chem Soc 2016;20:644–650; doi: 10.1016/j.jscs.2013.07.004.
65. Wang S, Zhou N. Removal of carbamazepine from aqueous solution using sono-activated persulfate process. Ultrason Sonochem 2016;29:156–162; doi: 10.1016/j.ultsonch.2015.09.008.
66. Lei Y, Cheng S, Luo N, et al. Rate constants and mechanisms of the reactions of $Cl^{\bullet}$ and $Cl_2^{\bullet-}$ with trace organic contaminants. Environ Sci Technol 2019;53(19):11170–11182; doi: 10.1021/acs.est.9b02462.
67. Wicktor F, Donati A, Herrmann H, et al. Laser based spectroscopic and kinetic investigations of reactions of the Cl atom with oxygenated hydrocarbons in aqueous solution. Phys Chem Chem Phys 2003;5(12):2562; doi: 10.1039/b212666d.
68. Alegre ML, Geronés M, Rosso JA, et al. Kinetic Study of the reactions of chlorine atoms and $Cl_2^{\bullet-}$ radical anions in aqueous solutions. 1. reaction with benzene. J Phys Chem A 2000;104(14):3117–3125; doi: 10.1021/jp9929768.
69. Wang P, Yang S, Shan L, et al. Involvements of chloride ion in decolorization of acid orange 7 by activated peroxydisulfate or peroxymonosulfate oxidation. J Environ Sci 2011;23(11):1799–1807; doi: 10.1016/S1001-0742(10)60620-1.

70. Potakis N, Frontistis Z, Antonopoulou M, et al. Oxidation of bisphenol A in water by heat-activated persulfate. J Environ Manage 2017;195:125–132; doi: 10.1016/j.jenvman.2016.05.045.
71. Lipczynska-Kochany E, Sprah G, Harms S. Influence of some groundwater and surface waters constituents on the degradation of 4-chlorophenol by the Fenton reaction. Chemosphere 1995;30(1):9–20; doi: 10.1016/0045-6535(94)00371-Z.
72. Liang C, Wang Z-S, Mohanty N. Influences of carbonate and chloride ions on persulfate oxidation of trichloroethylene at 20 °C. Sci Total Environ 2006;370:271–277; doi: 10.1016/j.scitotenv.2006.08.028.
73. Neta P, Huie RE, Ross AB. Rate constants for reactions of inorganic radicals in aqueous solution. J Phys Chem Ref Data 1988;17(3):1027–1284; doi: 10.1063/1.555808.
74. De Meyer T, Hemelsoet K, Van Speybroeck V, et al. Substituent effects on absorption spectra of pH indicators: An experimental and computational study of sulfonphthaleine dyes. Dyes Pigments 2014;102:241–250; doi: 10.1016/j.dyepig.2013.10.048.
75. Yang P, Liu J, Korshin GV, et al. New insights into the role of nitrite in the degradation of tetrabromobisphenol s by sulfate radical oxidation. Environ Sci Technol 2022;56(24):17743–17752; doi: 10.1021/acs.est.2c06821.
76. Gao X, Guo Q, Tang G, et al. Effects of inorganic ions on the photocatalytic degradation of carbamazepine. J Water Reuse Desalination 2019;9(3):301–309; doi: 10.2166/wrd.2019.001.
77. Xu X-R, Li X-Z. Degradation of azo dye orange g in aqueous solutions by persulfate with ferrous ion. Sep Purif Technol 2010;72:105–111; doi: 10.1016/j.seppur.2010.01.012.
78. Gu X, Lu S, Li L, et al. Oxidation of 1,1,1-trichloroethane stimulated by thermally activated persulfate. Ind Eng Chem Res 2011;50(19):11029–11036; doi: 10.1021/ie201059x.
79. Siegrist RL, Crimi M, Simpkin TJ, (eds). In situ chemical oxidation for groundwater remediation. SERDP/ESTCP Environmental Remediation Technology. Springer New York: New York, NY; 2011.; doi: 10.1007/978-1-4419-7826-4.
80. Ghauch A, Tuqan AM, Kibbi N, et al. Methylene blue discoloration by heated persulfate in aqueous solution. Chem Eng J 2012;213:259–271; doi: 10.1016/j.cej.2012.09.122.
81. Li S-X, Wei D, Mak N-K, et al. Degradation of diphenylamine by persulfate: Performance optimization, kinetics and mechanism. J Hazard Mater 2009;164(1):26–31; doi: 10.1016/j.jhazmat.2008.07.110.
82. Lahmar N, Djehiche M, Bachiri M. Removal of E110 from aqueous solution using heat-activated persulfate. Submited Eurasian J Chem 2024.
83. Bender JT, Petersen AS, Østergaard FC, et al. Understanding cation effects on the hydrogen evolution reaction. ACS Energy Lett 2023;8(1):657–665; doi: 10.1021/acsenergylett.2c02500.
84. Zhou D, Chen L, Li J, et al. Transition metal catalyzed sulfite auto-oxidation systems for oxidative decontamination in waters: A state-of-the-art minireview. Chem Eng J 2018;346:726–738; doi: 10.1016/j.cej.2018.04.016.
85. Xia X, Zhu F, Li J, et al. A review study on sulfate-radical-based advanced oxidation processes for domestic/industrial Wastewater Treatment: Degradation, Efficiency, and Mechanism. Front Chem 2020;8:592056; doi: 10.3389/fchem.2020.592056.
86. Park S-M, Lee S-W, Jeon P-Y, et al. Iron anode-mediated activation of persulfate. Water Air Soil Pollut 2016;227:462; doi: 10.1007/s11270-016-3169-4.
87. Zrinyi N, Pham AL-T. Oxidation of benzoic acid by heat-activated persulfate: Effect of temperature on transformation pathway and product distribution. Water Res 2017;120:43–51; doi: 10.1016/j.watres.2017.04.066.
88. Huang K-C, Zhao Z, Hoag GE, et al. Degradation of volatile organic compounds with thermally activated persulfate oxidation. Chemosphere 2005;61:551–560; doi: 10.1016/j.chemosphere.2005.02.032.
89. Yang C. Degradation of bisphenol A using electrochemical assistant Fe(II)-activated peroxydisulfate process. Water Sci Eng 2015;8:139–144; doi: 10.1016/j.wse.2015.04.002.
90. Mcheik AH, Jamal MME. Kinetic study of the discoloration of rhodamine b with persulfate, iron activation. J Chem Technol Metall 2013;357–365.
91. Yuan S, Liao P, Alshawabkeh AN. Electrolytic manipulation of persulfate reactivity by iron electrodes for trichloroethylene degradation in groundwater. Environ Sci Technol 2014;48(1):656–663; doi: 10.1021/es404535q.
92. Johnson RL, Tratnyek PG, Johnson RO. Persulfate persistence under thermal activation conditions. Environ Sci Technol 2008;42:9350–9356; doi: 10.1021/es8019462.
93. Yu X-Y, Bao Z-C, Barker JR. Free radical reactions involving $cl^{\bullet}$, $cl_2^{-\bullet}$, and $so_4^{-\bullet}$ in the 248 nm photolysis of aqueous solutions containing $S_2O_8^{2-}$ and Cl^-. J Phys Chem A 2004;108:295–308; doi: 10.1021/jp036211i.
94. Hayon E, McGarvey JJ. Flash photolysis in the vacuum ultraviolet region of sulfate, carbonate, and hydroxyl ions in aqueous solutions. J Phys Chem 1967;71(5):1472–1477; doi: 10.1021/j100864a044.

95. Huang K-C, Couttenye RA, Hoag GE. Kinetics of heat-assisted persulfate oxidation of methyl tert-butyl ether (MTBE). 2002;413–420.
96. Wojnárovits L, Takács E. Rate constants of sulfate radical anion reactions with organic molecules: A review. Chemosphere 2019;220:1014–1032; doi: 10.1016/j.chemosphere.2018.12.156.
97. Rehman F, Sayed M, Khan JA, et al. Oxidative removal of brilliant green by UV/S2O82–, UV/HSO5– and UV/H2O2 processes in aqueous media: A comparative study. J Hazard Mater 2018;357:506–514; doi: 10.1016/j.jhazmat.2018.06.012.
98. Chen L, Xue Y, Luo T, et al. Electrolysis-assisted UV/sulfite oxidation for water treatment with automatic adjustments of solution pH and dissolved oxygen. Chem Eng J 2021;403:126278; doi: 10.1016/j.cej.2020.126278.
99. Sirés I, Guivarch E, Oturan N, et al. Efficient removal of triphenylmethane dyes from aqueous medium by in situ electrogenerated Fenton's reagent at carbon-felt cathode. Chemosphere 2008;72(4):592–600; doi: 10.1016/j.chemosphere.2008.03.010.
100. Chen C-C, Fan H-J, Jan J-L. Degradation pathways and efficiencies of acid blue 1 by photocatalytic reaction with zno nanopowder. J Phys Chem C 2008;112:11962–11972; doi: 10.1021/jp801027r.
101. Jiang L, Zhang Y, Zhou M, et al. Oxidation of rhodamine b by persulfate activated with porous carbon aerogel through a non-radical mechanism. J Hazard Mater 2018;358:53–61; doi: 10.1016/j.jhazmat.2018.06.048.
102. Hammami S, Oturan N, Bellakhal N, et al. Oxidative degradation of direct orange 61 by electro-Fenton process using a carbon felt electrode: Application of the experimental design methodology. J Electroanal Chem 2007;610(1):75–84; doi: 10.1016/j.jelechem.2007.07.004.
103. Hori H, Yamamoto A, Hayakawa E, et al. Efficient decomposition of environmentally persistent perfluorocarboxylic acids by use of persulfate as a photochemical oxidant. Environ Sci Technol 2005;39(7):2383–2388; doi: 10.1021/es0484754.
104. Anipsitakis GP, Dionysiou DD, Gonzalez MA. Cobalt-mediated activation of peroxymonosulfate and sulfate radical attack on phenolic compounds. implications of chloride ions. Environ Sci Technol 2006;40(3):1000–1007; doi: 10.1021/es050634b.
105. Gokulakrishnan S, Parakh P, Prakash H. Degradation of malachite green by potassium persulphate, its enhancement by 1,8-dimethyl-1,3,6,8,10,13-hexaazacyclotetradecane nickel(II) perchlorate complex, and removal of antibacterial activity. J Hazard Mater 2012;213–214:19–27; doi: 10.1016/j.jhazmat.2012.01.031.
106. Ayoub ZA, Yazbeck OA, Jamal MME. Kinetic study of acid blue 1 discoloration with persulfate. J Chem Technol Metall 2017;52:812–824.